© Indian Academy of Sciences

OBSERVATIONAL FACILITIES

Effects of the moonlight on the operating parameters of the MACE γ-ray telescope: a feasibility study

M. KHURANA[1], K. K. SINGH[1,*] ⓘ, S. GODIYAL[1] and K. K. YADAV[1,2]

[1] Astrophysical Sciences Division, Bhabha Atomic Research Centre, Mumbai 400085, India.
[2] Homi Bhabha National Institute, Anushakti Nagar, Mumbai 400094, India.
*Corresponding author. E-mail: kksastro@barc.gov.in

Abstract. Major atmospheric Cherenkov experiment (MACE) is a very high-energy γ-ray telescope based on imaging atmospheric Cherenkov technique. The telescope has recently been installed at Hanle, Ladakh and results from its first light are expected very soon. The imaging atmospheric Cherenkov telescopes like MACE are usually operated during dark, clear and moonless nights and hence their duty cycle is limited to $\sim 10\%$ (1000 hours per year). Increasing the duty cycle of these telescopes is a challenging task in the field of ground-based very high-energy γ-ray astronomy. In this work, we study the feasibility of operating the MACE telescope under moderate moonlight to monitor the variable γ-ray sources in the sky as long as possible. We have developed a detailed methodology for estimating the contribution of moonlight as a function of its phase to the night sky background at the MACE site using the model of the brightness of moonlight proposed by Krisciunas & Shaefer (1991). The effect of additional background due to moonlight is examined on the various operational parameters such as anode current of the photomultiplier tubes in the camera, discriminator threshold, threshold energy and sensitivity of the MACE telescope. For the safe operation of the photomultiplier tubes under partial moonlight conditions, we estimate the gain in observation time or duty cycle of the telescope. It is found that if the strict requirements of the imaging atmospheric Cherenkov telescopes are relaxed by operating the photomultiplier tubes in the MACE camera at a lower gain or higher anode current and hence at a relatively higher energy threshold under moderate moonlight, a significant increase of $\sim 20\%$ in the effective observation time is expected every year for observations with the MACE telescope.

Keywords. Air shower—γ-ray astronomy—imaging atmospheric Cherenkov telescopes—moonlight.

1. Introduction

The imaging atmospheric Cherenkov telescopes (IACTs) have made very significant contributions in the development of ground-based γ-ray astronomy over the last three decades (Ong 1998; Aharonian *et al.* 2008; Hillas 2013; Horns 2016; Singh & Yadav 2021). The first seminal detection of the γ-rays from the Crab Nebula in 1989 using an IACT by the Whipple collaboration opened the window of a very exciting and productive area of research in the very high energy (VHE: $E > 20$ GeV) domain of the

electromagnetic spectrum (Weekes *et al.* 1989). The IACTs indirectly observe the VHE emission from the astrophysical sources by detecting the Cherenkov photons from the extensive air showers initiated by the cosmic γ-ray photons in the Earth's atmosphere. For a typical γ-ray shower, the lateral distribution of the Cherenkov photons on the ground is described by a nearly constant surface density within a blurry ring of radius ~ 125 m centered on the shower axis. An IACT placed inside this ring captures the image of the shower through the detection of Cherenkov photons emitted during the shower development in the atmosphere. The total Cherenkov light from a shower reaches the ground like a flash within a few nanoseconds. Therefore, IACTs are equipped with a

This article is part of the Special Issue on "Astrophysical Jets and Observational Facilities: A National Perspective".

large reflector and an array of fast photo-detectors at the focal plane for detecting the cosmic γ-rays. The number of Cherenkov photons emitted from a shower is in first-order proportional to the energy of the primary particle which initiates the shower. This suggests that the Earth's atmosphere can be considered as an open calorimeter for the indirect detection of the cosmic γ-rays from the ground.

The emission spectrum of Cherenkov photons (i.e., differential number of photons emitted per unit path length dx in the wavelength range λ and $\lambda + d\lambda$) for a particle of charge q and moving with relativistic velocity β (in units of c: speed of light in vacuum) is given by the Frank–Tamm relation (Yao *et al.* 2006)

$$\frac{d^2N}{dx\,d\lambda} = \frac{2\pi\alpha q^2}{\lambda^2}\left(1 - \frac{1}{\beta^2 n^2(\lambda)}\right), \qquad (1)$$

where α is the fine structure constant and $n(\lambda)$ is the refractive index of the dispersive medium. This indicates that the Cherenkov emission is dominant at short wavelengths and therefore the spectral intensity distribution has a peak in the UV wavelength band. However, the UV component of the emission Cherenkov spectrum is substantially modified due to strong atmospheric absorption (by ozone and aerosols) and scattering (mainly Rayleigh and Mie). Therefore, the observed Cherenkov spectrum on the ground is significantly different from the emitted one and peaks in the blue ($\lambda \sim 300$ nm) region of the electromagnetic spectrum. At wavelengths lower than UV, $n(\lambda)$ becomes less than one and therefore the particles no longer emit Cherenkov radiation. In detail, the observed spectral shape of the Cherenkov light is also sensitive to the zenith angle of observations and altitude of the observatory above sea level (asl). Therefore, detection of the Cherenkov light flash originating from the extensive air showers using ground-based IACTs is strongly affected by the isotropic light of the night sky (LONS) or night sky background (NSB) and artificial ambient light even during the dark night sky observations. Apart from the contributions due to zodiacal light, airglow, auroras, unresolved stars and galaxies to the background light in the night sky, the presence of moonlight also affects the observations with IACTs by increasing the noise level in the photo-detectors. The spectral distribution of the moonlight is different from that of the LONS and shows a better matching with the Cherenkov spectrum. Also, the observed Cherenkov spectrum, peaking in the blue wavelength region, significantly differs from the LONS which dominantly contribute to the higher wavelength band. This suggests that the photo-detectors employed

in IACTs must be sensitive enough to discern the feeble Cherenkov light flash over the LONS and moonlight. At the same time, statistical fluctuations of the LONS and moonlight must be rejected on the hardware level itself during the observations.

IACTs generally use photomultiplier tubes (PMTs) as photon sensors in the camera for detecting the Cherenkov light during dark nights. The PMTs may suffer significant aging or can be damaged due to excess or high background light level. However, PMTs can be used for observations during brighter conditions by reducing their gain (lowering the high voltage). This also degrades the performance of PMTs if the gain is reduced significantly. Therefore, the presence of moonlight in the night sky can result in physical damage to the PMTs as well as contamination to the Cherenkov light recorded by the IACTs. The only motivation for observations using IACTs under moonlight conditions is the enhancement of the duty cycle, which is very important for monitoring the γ-ray sources with variability at different timescales ranging from a few minutes to years (Singh & Meintjes 2020). Existing state-of-the-art IACTs like MAGIC and VERITAS have been designed to allow for observations under moonlight conditions. The MAGIC telescopes, at La Palma in the Canary Islands, are operated under non-standard hardware configurations when the Moon is present in the sky (Ahnen *et al.* 2017). This includes a reduction in PMT gain by a factor ~ 1.7 for standard settings or using UV-bandpass filters in front of the camera. It has resulted in increasing the total duty cycle of MAGIC up to $\sim 40\%$. The VERITAS IACTs, at the Fred Lawrence Whipple Observatory in southern Arizona, are operated under the bright moonlight in two observing modes, first by reducing the high voltage applied to the PMTs and, second, by adding UV-bandpass filters to the cameras (Archambault *et al.* 2017). About $\sim 30\%$ gain in observation time has been achieved in a year for the VERITAS telescopes. In the present work, we study the plausible impact of moonlight on the operating parameters of the MACE γ-ray telescope and discuss the partial moonlight conditions for the safe operation of the telescope at Hanle, Ladakh, India.

2. The MACE telescope

The major atmospheric Cherenkov experiment (MACE) is an IACT located at Hanle (32.8°N, 78.9°E, 4.3 km above sea level) in Ladakh. The telescope has been recently commissioned and is moving towards its regular science observations. The entire telescope electronics as

well as its operation is powered by a 240 kW on-site solar power station. A recent photograph of the MACE telescope is depicted in Figure 1 and its salient features are summarized in Table 1. It has been designed for exploring the γ-ray sky with a low energy threshold and high flux sensitivity (Koul 2017; Singh & Yadav 2021). Equipped with a quasi-parabolic reflector of 21 m diameter and 25 m focal length, MACE is expected to observe high energy γ-ray emission from the celestial sources in the energy range of 20 GeV–5 TeV (Borwankar *et al.* 2020). The alt-azimuth mount of MACE provides a very fast repositioning of the telescope in any direction in the sky. The imaging camera at the focal plane is composed of 1088 PMTs with low gain and high quantum efficiency. One of the unique features of the MACE camera is its modular structure with 68 camera integrated modules (CIMs). Each module consists of 16 PMTs with in-house front-end electronics for detecting the Cherenkov light flash. A domino ring sampler version 4 (DRS4) developed by Stefan Ritt, Paul Scherrer Institute, Switzerland is employed for a very fast sampling of the signal from the PMTs. It helps in reducing the contamination of LONS. The representative Cherenkov spectrum (defined in Equation 1) and measured differential photon flux due to LONS at Hanle in four wavelength bands are shown in Figure 2(a) and (b) respectively. The LONS values are derived from the actual measurements in U, B, V and R bands at the Indian Astronomical Observatory (IAO), Hanle, during the period 2003–2008 (Stalin *et al.* 2008). A simple parabolic fit to the measured flux points reported in Figure 2(b) suggests that the contribution due to LONS dominates at wavelengths above 450 nm whereas the Cherenkov spectrum peaks at ∼ 350 nm. The integral photon flux due to LONS at the Hanle site is ∼ 10^{12} ph m^{-2} s^{-1} sr^{-1}. It can be detected by each

Table.1. Important features of the MACE telescope.

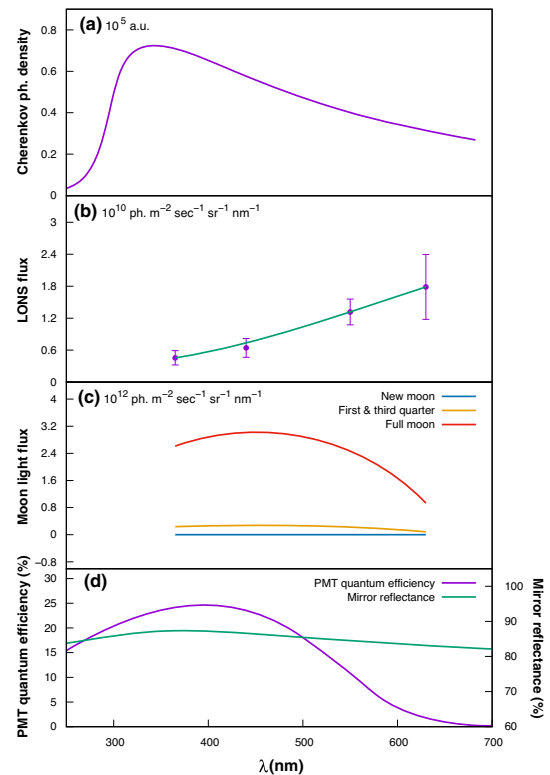|	
f-number	1.2
Reflector area	340 m^2
Weight	180 ton
Camera size	2.2 × 1.3 m
Point spread function	45 mm
Energy threshold	20 GeV
Integral sensitivity	2.7% (Crab)
Field of view	4.36° × 4.03°
Trigger rate	1 kHz
Energy resolution	25%
Angular resolution	0.125°
Tracking accuracy	20 arc-sec
Tracking speed	3° s^{-1}
Solar power supply	240 kW

Figure 2. (a) Representative Cherenkov spectrum (Equation (1), (b) LONS measured at Hanle during moonless nights, (c) photon flux due to moonlight during different lunar phases at Hanle and (d) quantum efficiency of PMTs used in MACE camera and reflectance of the metallic mirror facets as a function of wavelength.

Figure 1. MACE γ-ray telescope at Hanle, Ladakh, India.

PMT in the MACE camera at a single-channel rate (SCR) of ∼ 100 MHz during moonless nights. The SCR is defined as the trigger rate of a single PMT due to

fluctuations in LONS, Cherenkov light from an air shower in the atmosphere or after-pulsing of the PMTs. It depends on the value of the pre-defined single-channel discrimination threshold (DT) fixed in the night observations. This is expected to increase significantly due to the presence of partial moonlight during the ground-based observations of the potential γ-ray sources.

3. The Moon-Earth system

In our planetary system, the Moon is the natural satellite of the Earth. It revolves around the Earth in a synchronous orbit with an orbital eccentricity of ~ 0.055. The orbit of the Moon is inclined at an angle of $\sim 5°$ against the ecliptic inclination as seen from the Earth. The inclined orbit and small variations in the viewing angle from the Earth allow us to see $\sim 60\%$ of the Moon's surface. The minimum and maximum distances of the Moon from the Earth are 357643 km (perigee) and 406395 km (apogee) respectively. The angular size of the Moon as seen from the Earth is $\sim 0.5°$ in the celestial sphere[1]. The Moon does not emit any light or radiation by itself, but only reflects mostly sunlight by the lunar surface. The reflection of light from the lunar surface is quite different from that of a Lambertian surface. A fit to the lunar albedo in the wavelength range 240–800 nm is given by (Dobber *et al.* 1998)

$$a(\lambda) = 1 + 2.1 \times 10^{-4}(\lambda - 5500 \text{ Å}) \qquad (2)$$

and the lunar V-magnitude is expressed as

$$V_m(\alpha) = -12.73 + 0.026|\alpha| + 4 \times 10^{-9}\alpha^4, \qquad (3)$$

where α is the phase angle of the Moon or lunar phase. It is defined as the angle between the Sun and the Earth as viewed from the Moon. The orbital period of the Moon around the Earth is 27.3 days and the orbital period of the Earth around the Sun is 365.25 days (one astronomical year). This corresponds to one synodic period of 29.5 days. The Sun-Earth-Moon system cannot be in the same constellation after one year due to the ecliptic inclination of the orbit of the Moon. Although the same side of the Moon is always seen from the Earth, it has different phases corresponding to the fractional illumination due to relative positions of the Sun, the Earth and the Moon. The illuminated fraction of the Moon is a simple function of α and is estimated as

$$F = \frac{1 + \cos\alpha}{2}. \qquad (4)$$

---

[1]http://nssdc.gsfc.nasa.gov/planetary/factsheet/moonfact.html.

Therefore, the illuminated fraction of the Moon is correlated with its celestial position as seen from the Earth. There are mainly four phases of the Moon generally referred to like the new, first-quarter, full and third-quarter.

- New Moon ($F = 0, \alpha = 180°$), the Sun and the Moon are in conjunction and the back-side of the Moon is illuminated. The new Moon is only visible during the daytime and invisible during night (the Sun and the Earth are on the opposite sides of the Moon).
- First-quarter Moon ($F = 0.5, \alpha = 90°$), half of the Moon is illuminated as seen from the Earth. In the northern hemisphere, the right side of the Moon is visible as the Moon rises in the middle of the day and sets during midnight.
- Full Moon ($F = 1.0, \alpha = 0°$), the Sun and the Moon are on the opposite sides of the Earth. All the Moon's surface is visible from the Earth and appears to be fully illuminated for a couple of days before and after the full Moon.
- Third-quarter Moon ($F = 0.5, \alpha = 90°$), the other half of the Moon is illuminated compared to the first-quarter. On the day of the third or last quarter, the Moon rises approximately at the midnight and sets in the middle of the day.

All intermediate values of α between $0°$ and $180°$ are possible and enable different phases of the Moon to be seen from the Earth. If the Moon is visible, the brightness of moonlight dominates over the LONS.

4. Model for Moon brightness

Complete theoretical modeling of the brightness due to the moonlight (B_m) depends on many parameters such as the intensity of the moonlight as a function of the lunar phase, properties of the Earth's atmosphere, zenith distance of the Moon, and the separation between the source under observation and the Moon. The total brightness of the night sky background at any geographical position on the Earth in the presence of the Moon in the sky can be expressed as

$$B(\alpha, \rho, \lambda, Z_m, Z_s) = B_0(\lambda) + B_m(\alpha, \rho, \lambda, Z_m, Z_s), \qquad (5)$$

where $B_0(\lambda)$ corresponds to the brightness due to LONS (Figure 2b) and $B_m(\alpha, \rho, \lambda, Z_m, Z_s)$ is the additional brightness contribution from the moonlight. ρ is the angular separation between the Moon and the source being observed by an IACT. Z_m and Z_s are the
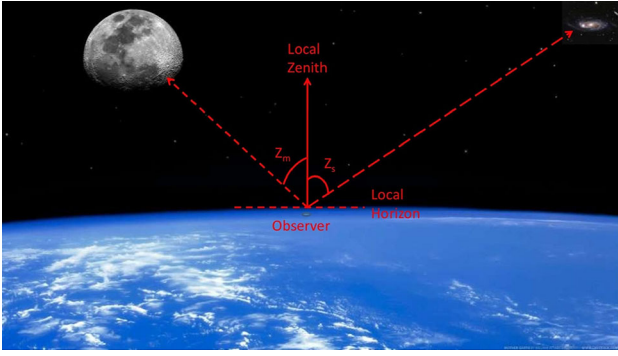
Figure 3. Representative diagram showing the relative positions of the Earth, Moon and γ-ray source.

zenith angles of the Moon and γ-ray source respectively. These parameters are defined in Figure 3. From the simple trigonometric relations, the separation between the Moon and sky position associated with a source is given by

$$\cos \rho = \sin Z_s \sin Z_m \cos(A_m - A_s) + \cos Z_s \cos Z_m, \tag{6}$$

where A_m and A_s are azimuth of the Moon and source respectively. Estimation of $B_m(\alpha, \rho, \lambda, Z_m, Z_s)$ in the present work is inspired by the formalism proposed in (Krisciunas & Shaefer 1991) for the brightness of moonlight in V-band. The wavelength dependence of lunar albedo (Equation 2), solar flux and atmospheric scattering can be taken into account to extrapolate the brightness of the Moon beyond the V-band (Equation 3). Therefore, the wavelength-dependent brightness of moonlight for $Z_m < 90°$ is expressed as

$$\begin{aligned} B_m(\alpha, \rho, \lambda, Z_m, Z_s) &= a(\lambda) \times \frac{F_s(\lambda)}{F_s(5500 \text{ Å})} \\ &\times 10^{-0.4k(\lambda)X(Z_m)} \times 10^{[-0.4(V_m(\alpha)+16.37)]} \\ &\times (1 - 10^{[-0.4k(\lambda)X(Z_s)]}) \times f(\rho, \lambda), \end{aligned} \tag{7}$$

in units of *nano-Lamberts* ($1 \text{ nL} = 1.12 \times 10^{-19} \text{ ergs}^{-1}$ cm^{-2} arc-sec^{-1} Å^{-1}). If the Moon is below the horizon ($Z_m > 90°$), right-hand side of Equation (7) vanishes. In the above equation, $F_s(\lambda)$ corresponds to the wavelength-dependent solar flux in the visible range and $k(\lambda)$ is the mean extinction coefficient (in units of magnitude/air-mass) in different wavelength bands. The optical path length along a line of sight in units of air masses (X) for atmospheric radiation is given by (Krisciunas & Shaefer 1991)

$$X(Z) = (1 - 0.96 \sin^2 Z)^{-0.5}, \tag{8}$$

where Z is the zenith distance. The scattering function, $f(\rho)$, takes into account the complex calculations involved in the complex scattering problem of the moonlight and strongly depends on the scattering angle. The scattering angle is assumed to be the same as the separation angle (ρ). The scattering of moonlight can be described by the combination of Rayleigh scattering by the atmospheric molecules (mainly oxygen and nitrogen) with size significantly larger than λ and Mie scattering by the particles (dust and aerosols) of dimension similar to λ (Chandrasekhar 1950; Bernstein *et al.* 2002). The intensity of scattered moonlight is described by $f(\rho)$ which is expressed as

$$f(\rho, \lambda) = f_R(\rho, \lambda) + f_M(\rho, \lambda), \tag{9}$$

where $f_R(\rho, \lambda)$ and $f_M(\rho, \lambda)$ represent contributions to the total scattering function corresponding to the Rayleigh and Mie scattering respectively. Taking into account the wavelength dependence of the respective scattering cross-section, $f_R(\rho, \lambda)$ and $f_M(\rho, \lambda)$ can be expressed as (Krisciunas & Shaefer 1991; Patat 2003; Nordsieck 2004)

$$\begin{aligned} &f_R(\rho, \lambda) \\ &= 10^{5.36}(1.06 + \cos^2 \rho) \left(\frac{\lambda}{5500 \text{ Å}}\right)^{-4} \left(\frac{k(5500 \text{ Å})}{k(\lambda)}\right) \end{aligned} \tag{10}$$

and

$$\begin{aligned} &f_M(\rho, \lambda) \\ &= 10^{6.15-(\rho/40)} \left(\frac{\lambda}{5500 \text{ Å}}\right)^{-0.5} \left(\frac{k(5500 \text{ Å})}{k(\lambda)}\right), \end{aligned} \tag{11}$$

in units of nL. Using Equations (8)–(11) in Equation (7) and performing appropriate unit conversions, the photon flux due to moonlight is given by

$$\begin{aligned} &\phi_{\text{moon}}(\alpha, \rho, \lambda, Z_m, Z_s) \\ &= 0.293 \times B_m(\alpha, \rho, \lambda, Z_m, Z_s) \times \lambda(\text{Å}), \end{aligned} \tag{12}$$

in units of ph cm^{-2} s^{-1} sr^{-1} Å^{-1}. The variation of ϕ_{moon} as a function of λ corresponding to the different lunar phases for an arbitrary separation angle ($\rho = 9°$) is presented in Figure 2(c). It is observed that the contribution of the moonlight photon flux to the night sky background strongly depends on the lunar phase.

The values of wavelength-dependent extinction coefficient $k(\lambda)$ and normalized solar flux used in this work for the Hanle site are reported in Table 2.

Table.2. Mean extinction coefficient measured at Hanle and solar flux normalized at $\lambda = 5500$ Å.

	3650 Å (U)	4400 Å (B)	5500 Å (V)	6300 Å (R)
$k(\lambda)$	0.36	0.21	0.12	0.09
$\dfrac{F_s(\lambda)}{F_s(5500\ \text{Å})}$	0.5585	0.9727	1.0000	0.7500

Table.3. Characteristics of the PMTs used in the MACE camera.

Window material	UV glass (refractive index: 1.48)
Photocathode	Bialkali (spectral range: 220–680 nm)
Dynodes	SbCs (6-stage, circularly focused)
Rise time	2 ns (multi electron)
Quantum efficiency	26% (peak)
Gain	Low gain ($\sim 10^4$)
Dark current	0.5–2.5 nA (at 20°C)
Anode current	100 μA (maximum)

5. MACE parameters under moonlight observations

The Hanle site offers an annual average of about 260 uniformly distributed spectroscopic nights round the year with good sky coverage for γ-ray observations. This is one of the important criteria for the selection of the MACE telescope site at Hanle. The duty cycle of the MACE telescope can be further increased by taking into account the presence of moonlight during night sky observations. The detection system of the MACE telescope mainly comprises a large optical reflector of area ~ 340 m^2 and an imaging camera equipped with 1088 PMTs at the focal plane. The reflector is made of 1424 high optical quality metallic mirror facets of area ~ 0.25 m^2 each. These mirrors facets have been indigenously developed using diamond turning technology and exhibit an average reflectance above 80% in the wavelength range of 250–700 nm. A representative measurement of the reflectance for the mirror facets used in the MACE reflector is shown in Figure 2(d). The PMTs employed in the MACE camera are Electron Tubes Enterprises Limited made with the 9117WSB series. The important characteristics of these PMTs are summarized in Table 3. From the features described in Table 3, it is obvious that the PMTs chosen for the MACE camera have relatively low gain. This has the advantage of operating the PMTs under the high level of night sky background light. Effects of the contributions from the moonlight to the night sky background on the important operating parameters of the telescope are discussed.

5.1 *PMT anode current*

The anode current for each PMT is strictly monitored throughout the observations with IACTs for the safe operation of the imaging camera. It can be calculated from the photon-electron flux in each PMT due to the detection of night sky background light. The constant nature of LONS and moonlight for a given lunar phase

result in a high direct current (DC) as the anode current of each PMT. From the appropriate information regarding the spectral distributions given in Figure 2, the photo-electron flux in the PMT is given by

$$\phi_{\text{pe}} = \int_{\lambda_{\min}}^{\lambda_{\max}} \phi(\lambda)\eta_{\text{PMT}}(\lambda)\eta_{\text{mir}}(\lambda)d\lambda, \tag{13}$$

in units of pe cm^{-2} s^{-1} sr^{-1}. $\phi(\lambda)$ represents contributions associated with the differential spectra of LONS ($(\phi_0(\lambda))$) as shown in Figure 2(b) and the moonlight ($\phi_{\text{moon}}(\lambda)$) as defined in Equation (12). $\eta_{\text{PMT}}(\lambda)$ and $\eta_{\text{mir}}(\lambda)$ are the quantum efficiency of the PMT and mirror reflectance, respectively (Figure 2). Therefore, the anode current of each PMT can be expressed as

$$I(\mu A) = \frac{\phi_{\text{pe}} \times \Omega \times A \times G}{6.25 \times 10^{12}}, \tag{14}$$

where Ω is the solid angle of the PMT, A is the reflector area of the telescope and G is the gain of PMT. If 2θ is the angular size of the PMT, the solid angle subtended by it is given by

$$\Omega = 2\pi(1 - \cos\theta). \tag{15}$$

For the MACE telescope, $G \sim 10^4$, $\theta = 0.125°$, $A = 340$ m^2. Using these parameters, the anode current of the PMT in the MACE camera is estimated to be ~ 1.3 μA corresponding to the LONS. This anode current starts increasing sharply due to the presence of the moonlight. Variation of the anode current as a function of the Moon phase for different separation angles is shown in Figure 4(a). It is observed that the PMTs in the MACE camera can be used with a maximum anode current of ~ 30 μA following the strict requirements of their safe operation during the observations. If the Moon phase angle is expressed as $-180° \leq \alpha \leq 180°$ during the Moon cycle in a month, the MACE telescope can be safely operated up to a lunar phase of $\pm 60°$ for smaller separation angles
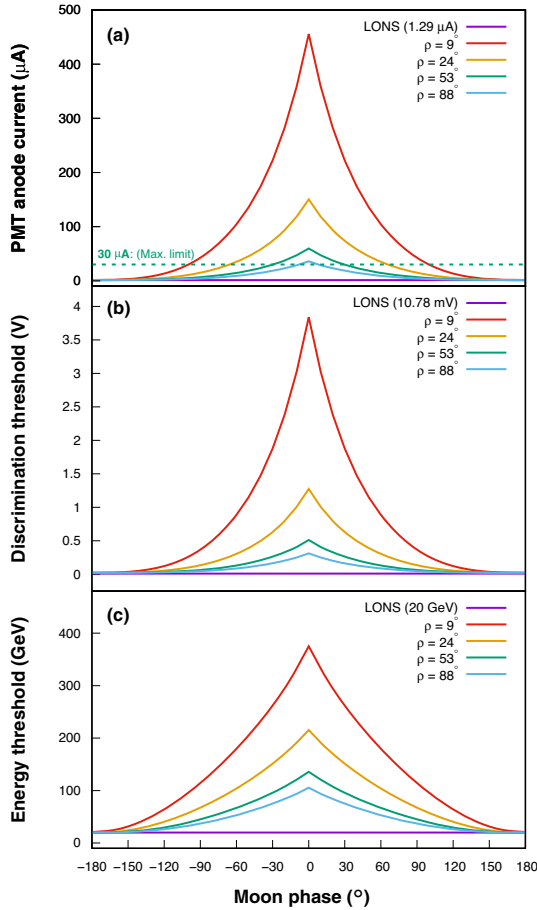
Figure 4. Operating parameters of the MACE telescope under moonlight conditions.

between the Moon and γ-ray source. If the separation angle is beyond $50°$, the telescope can be employed for γ-ray observations even during full Moon conditions using suitable hardware systems like an anode current handler in the camera.

5.2 *Discrimination threshold*

A voltage pulse is generated corresponding to the anode current of each PMT. If the pulse height exceeds a certain threshold (DT), an output signal is produced. The value of DT is determined from the statistical fluctuations of the LONS and is used as a first background rejection on a hardware level in IACTs. The pulse height associated with DT is defined as

$$V_{DT} = I \times R \times g_1 \times g_2, \qquad (16)$$

where R is the resistance at the output of PMT, g_1 and g_2 are the gain of pre-amplifier and secondary amplifier respectively in the circuit. The value of V_{DT} can be

adjusted individually for each PMT in the camera and determines the SCR during observations. In case of the MACE camera, $R = 50\ \Omega$, $g_1 \sim 11$ and $g_2 = 1.2 - 14$ correspond to $V_{DT} \sim 10$ mV for LONS. The moonlight increases the value of V_{DT} significantly as shown in Figure 4(b). The behavior of DT as a function of the lunar phase is similar to that of the anode current. A value of V_{DT} above 100 mV is not desirable as this can result in the non-detection of Cherenkov pulses coming from the low energy showers. Therefore, the value of V_{DT} is properly optimized through the Monte-Carlo simulations of an IACT and fluctuations due to the electronic noise in the data acquisition system. It should be assigned a value which can significantly minimize the false triggers in the camera due to fluctuations in the LONS as well as the moonlight during observations. An event trigger corresponding to the Cherenkov light flash is generated in the camera of an IACT when the pulse amplitudes of a few neighboring PMTs cross the DT value within a predefined time window of few nanoseconds.

5.3 *Energy threshold*

The energy threshold of an IACT is characterized as the minimum detectable energy of the primary γ-rays originating from the Crab Nebula. It strongly depends on the level of night sky background light at an astronomical site among other factors related to a telescope. For a given IACT, the energy threshold is defined as (Fegan 1997)

$$E_{th} \propto \sqrt{\frac{\phi \Omega \tau}{\eta_{PMT} A}}, \qquad (17)$$

where $\phi = \phi_0 + \phi_{moon}$, is the total photon flux of the night sky background light and τ is integration time of the Cherenkov pulse. This indicates the lower energy threshold of an IACT can be achieved by minimizing the contribution of the background light and increasing the area of the light collector. But, the presence of moonlight increases the level of night sky background light and hence the energy threshold of an IACT. The normalized energy threshold under moonlight conditions for the dark conditions is given by

$$\frac{E_{th}}{E_0} = \sqrt{1 + \frac{\phi_{moon}}{\phi_0}}, \qquad (18)$$

where E_0 is the energy threshold corresponding to the LONS only. For the MACE telescope, Monte-Carlo simulations suggest $E_0 \sim 20$ GeV (Borwankar *et al.*

2020). As depicted in Figure 4(c), the energy threshold of MACE may increase up to ~ 100 GeV due to the effects of the additional moonlight if the telescope is safely operated under partial moonlight conditions. An increase in the energy threshold for large IACTs like MACE is not desirable as they have been designed for γ-ray observations at lower energies. E_{th} is linearly correlated with the DT values set up during observations. Increased DT values or higher energy threshold may lead to a decrease in the overall sensitivity of an IACT, which is defined as the minimum observation time required to detect a statistically significant γ-ray signal over huge cosmic-ray background (signal-to-noise ratio ~ 5) from the Crab Nebula like sources. Detailed estimation of the sensitivity of the MACE telescope under partial moonlight conditions is beyond the scope of this work.

6. Discussion and conclusion

IACTs are generally deployed to monitor the γ-ray emission from the astrophysical sources in the so-called ON/OFF observation mode. In this mode, equal time is dedicated for observing a target γ-ray source (ON, assuming the source is in the camera center) and a background region in the sky without any candidate source (OFF, for estimating the isotropic cosmic ray background). This additional observation time for OFF observation along with the strict requirement of IACT operations under dark and clear nights limits the available time of observations about 1000 hours per year. However, the present study suggests that the MACE telescope can be safely used to observe the γ-ray sources under partial moonlight conditions. If T_0 is the time available for observations under dark conditions with LONS only and T is observation time during partial moonlight conditions in a year, % gain in observation time is given by (Dawson & Smith 1996)

$$T_{gain} = \frac{T - T_0}{T_0} \times 100, \tag{19}$$

where $T_0 \sim 18\%$. T is related to the illuminated fraction of the Moon (F). The gain in observation time for the MACE telescope estimated from the feasibility study in the present work for the representative arbitrary separation angles between a γ-ray source and the Moon is summarized in Table 4. We conclude that it is safe to operate the MACE telescope under the

Table.4. Gain in observation time per year for the MACE telescope under partial moonlight operation.

α	ρ	T_{gain} (%)
$10°$	$88°$	97
$30°$	$53°$	65
$70°$	$24°$	31
$100°$	$9°$	14

partial moonlight conditions taking into account the following effects:

- Individual PMTs in the MACE camera can be safely operated at an anode current up to 30 μA.
- The discrimination threshold value up to 100 mV can be set during observations.
- Energy threshold of the telescope may increase up to 100 GeV at the cost of a decrease in the sensitivity.

Due to the above effects, the data analysis procedure for the MACE telescope will be significantly changed. Therefore, observations of the Crab Nebula under the moonlight conditions are essential for quantifying these effects on the telescope performance. Some other ways for allowing IACTs to operate under moonlight conditions are (i) restricting the sensitivity of PMTs to the near UV wavelengths below 350 nm, (ii) using the solar-blind PMTs which are sensitive below 400 nm and (iii) employing blue-light blocking filter next to the PMTs (Chantell *et al.* 1997).

References

Aharonian F. *et al.* 2008, Rep. Prog. Phys., 71, 096901
Ahnen M. L. *et al.* 2017, APh, 94, 29
Archambault S. *et al.* 2017, APh, 91, 34
Bernstein R. A. *et al.* 2002, ApJ, 571, 85
Borwankar C. *et al.* 2020, NIMP A, 953, 163182
Chandrasekhar S. 1950, Radiative Transfer (Oxford: Clarendon)
Chantell M. C. *et al.* 1997, APh, 6, 205
Dawson B., Smith A. 1996, GAP-96-034

Dobber M. R. *et al.* 1998, Appl. Opt., 37, 7832
Fegan D. J. 1997, JPhG, 23, 1013
Hillas A. M. 2013, APh, 43, 19
Horns D. 2016, JPhCS, 718, 022010
Koul R. 2017, Curr. Sci., 113, 691
Krisciunas K., Shaefer B. 1991, PASP, 103, 1033
Nordsieck K. 2004, SALT-3172AS0005

Ong R. A. 1998 Phys. Rep., 305, 93
Patat F. 2003, A&A, 400, 1183
Singh K. K., Meintjes P. J. 2020, AN, 341, 713
Singh K. K., Yadav K. K. 2021, Universe, 7, 96
Stalin C. S. *et al.* 2008, BASI, 36, 111
Weekes T. C. *et al.* 1989, ApJ, 342, 379
Yao W. M. *et al.* 2006, JPhG, 33, 1